Viewing Phobos and Deimos for Navigating Mariner 9

T. C. DUXBURY,* G. H. BORN,* AND N. JERATH†
Jet Propulsion Laboratory, Pasadena, Calif.

A new on-board optical navigation data technique has been successfully demonstrated on Mariner 9. Science TV pictures of Phobos and Deimos against star fields were used in the real time navigation process for inserting Mariner 9 into orbit about Mars. Real time and post flight evaluation results have shown that the satellite/star data taken by Mariner 9 surpassed preflight accuracy predictions. Orbital insertion could have been achieved using only optical data to determine encounter parameters. The use of a science TV camera to obtain this data was successfully demonstrated. Stars as dim as 9th magnitude were detected and measurement accuracies of 3 arc sec (1σ) were achieved.

I. Introduction

A NEW on-board optical navigation data technique has been proposed for use on outer planet missions.[1] The technique uses a television camera to view natural satellites against a star background during planetary approach. An in-flight pointing and geometric calibration of the TV was proposed to obtain an optical data accuracy of 5 arc sec (1σ).[2] Stars as dim as 8th magnitude must be detectable to insure star availability for any arrival geometry. The Mariner Mars 1971 mission offered a unique opportunity to demonstrate this new technique during flight operations before committing future missions to its use. Every aspect of this technique was demonstrated to be feasible during MM'71. Based on this success, the Viking and Mariner Jupiter/Saturn missions have committed to use optical navigation data during approach operations. This paper presents the results of the post flight evaluation of the satellite/star on-board optical navigation data taken during the approach phase of MM'71.

Prior to approach operations, the TV had been calibrated and had detected 9th magnitude stars. During real time mission operations, Deimos/star data were combined with radio tracking data to produce the most accurate trajectory estimate ever obtained during interplanetary flight operations. An optical data accuracy of 3 arc sec (1σ) was achieved. It was found that optical navigation alone would have been adequate to insert Mariner 9 into orbit about Mars within mission accuracy requirements. Only one star per picture was required to yield the full accuracy potential of the optical data. A few days of radio Doppler data combined with the optical data yielded the full accuracy potential of the combined optical/radio data. TV satellite data were found to be superior over Mars limb data for approach navigation. Also, star images in flight pictures were sufficient to perform the calibration of the TV for navigation, independent of other ground or flight calibration data.

Details of the TV calibration for navigation are given in Refs. 3 and 4. Details of the data processing software and mission operations are given in Ref. 5.

Presented as Paper 72-927 at the AIAA/AAS Astrodynamics Conference, Palo Alto, Calif., September 11–12, 1972; submitted October 30, 1972; revision received August 27, 1973. This paper presents the results of work carried out at the Jet Propulsion Laboratory, California Institute of Technology under Contract NAS 7-100, approved by the National Aeronautics and Space Administration.

Index category: Spacecraft Navigation, Guidance, and Flight Path Control Systems.

* Member of Technical Staff.
* Member of Technical Staff.
† Research Engineer.

II. Source of Optical Data

The narrow angle science television camera was the source of the optical navigation observations for MM'71. The narrow angle TV has a 500 mm focal length with f/2.5 Schmidt-Cassegrain optics. A selenium-sulfur vidicon tube with a 7×9 reseau grid was used. A 9.6×12.5 mm area on the vidicon target was scanned with a resolution of 700 scan lines and 832 picture elements (pixels) per scan line. The active area of the vidicon target gave a $1.1 \times 1.4°$ field of view with an angular resolution of 6 arc sec per pixel. The video intensity of each pixel was digitized to 9 bits. Each picture element, therefore, would be defined by its pixel number (1 to 832), its line number (1 to 700) and its intensity (0 to 511).

The narrow angle camera can be shuttered on intervals of 84 sec allowing sufficient time for a picture to be read out and recorded. Exposures may be ground commanded from 0.006 to 6.144 sec, enabling stars as dim as 9th magnitude to be detected.

III. Optical Data Errors

Optical data errors are classified as instrument and model errors. Instrument errors include TV distortions, TV pointing errors, image center-finding errors, and random measurement errors. TV distortion errors corrupt the relative geometry of images within a picture. TV distortion causes image location errors of a few pixels near the center of the vidicon to many

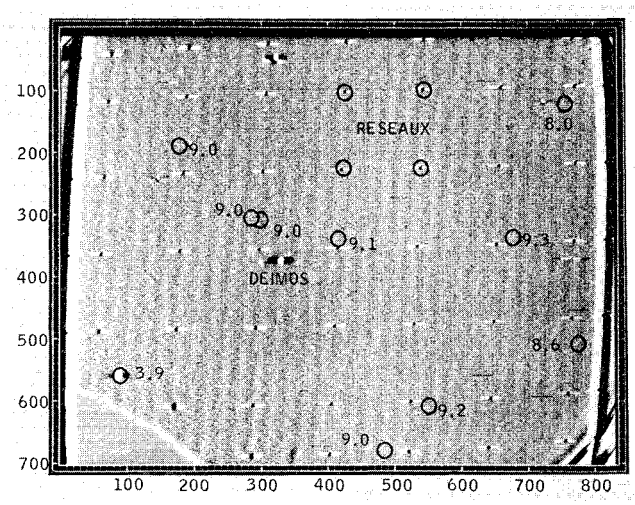

Fig. 1 Approach Deimos picture.

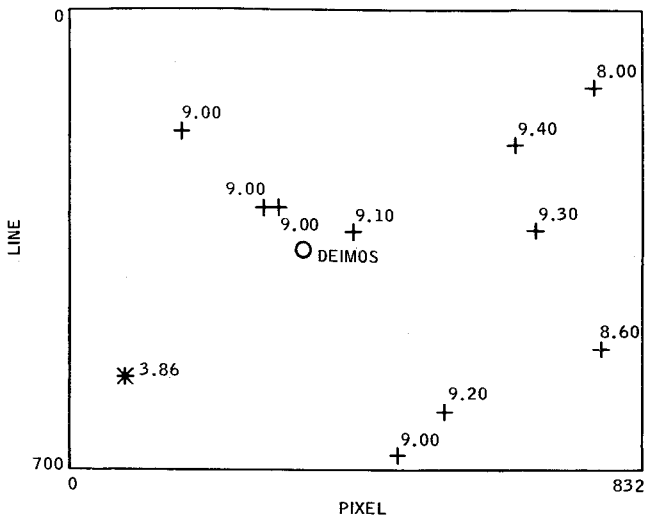

Fig. 2 Predicted approach Deimos picture.

pixels near the edges of the vidicon. This distortion is accurately modeled as a polynomial of the radial distance from the center of the vidicon.[2] Either reseau or star images may be used to calibrate TV distortion. Distortion from the optics is negligible.

TV pointing errors cause a global shift of all images in a picture. TV pointing errors, caused by imperfect knowledge of TV pointing directions at shutter times, can be eliminated if stars with known directions are included in the picture.

Image center-finding errors result when dealing with finite size images such as those of Deimos and Phobos. Also, limit cycle motion during exposure, diffraction in the optics, and blooming of saturated images combine to yield finite size images. These center-finding errors are of pixel or subpixel magnitude for Phobos and Deimos.

Model errors include satellite ephemeris errors as well as planet gravity and spin axis errors. Deimos and Phobos ephemerides were modeled by a first-order analytic theory.[6] For MM'71, the effects of these model errors were minimized by including Deimos and Phobos orbital elements and the mass and spin axis direction of Mars as estimated parameters.

IV. Data Types and Content

Optical navigation observables were defined as the image locations (pixel and line numbers) of Deimos, Phobos, stars, and reseaux. An approach picture is shown in Fig. 1 which has the images of Deimos, ten stars of magnitude 3.9 to 9.2, and the 7×9 reseau grid. Stray light from Mars is seen in the lower left portion of the picture. The picture was enhanced to bring out the dim images. Figure 2 is a computer drawn version of the picture which is used to distinguish the star pattern from noise or vidicon blemishes.

Reseau images were used to compute the coefficients of a TV distortion polynomial to subpixel accuracy. Star images were used to compute the TV pointing direction to an accuracy commensurate with the TV resolution of 3 arc sec (1σ). Star images were also used postflight to yield an equally accurate determination of TV distortion as reseaux. Satellite images contained information on satellite ephemerides, the spacecraft trajectory, and Mars gravity potential and spin axis direction.

The reseau data used in TV distortion calibration for real time operations and a majority of postflight evaluation was obtained from pictures taken about a month before orbit insertion. With the TV distortion being stable to subpixel level from prelaunch through flight, no additional reseau data was processed during Mars approach. Star and reseau data, independent of spacecraft trajectory for this application, could be either processed separately or combined with the satellite data processing.

V. Approach Pictures

During the 3-day approach period prior to the insertion of Mariner 9 into orbit about Mars, three Preorbital Science picture sequences (POS I, II, and III) were taken (Fig. 3). Each POS sequence covered a 24-hr period with 31 pictures being recorded aboard Mariner 9 and then transmitted to Earth during a 3-hr period near Goldstone (Deep Space Station 14) zenith. Since orbit insertion was performed early in the Goldstone tracking window, the POS III pictures were played back after orbit insertion. With only POS I and POS II pictures to be played back prior to insertion, all 13 optical navigation pictures in these two sequences were targeted to Deimos. This allowed its ephemeris uncertainty to be reduced to a level which would not seriously degrade the approach spacecraft trajectory estimates. The small angular separation of Phobos and Mars during this period made Phobos an undesirable target because of possible Mars stray light interference. The eight pictures in POS III were divided between five of Deimos and three of Phobos.

The positions of Deimos as viewed from Mariner 9 against the star background are shown in Fig. 4. During approach operations, the first Deimos picture was lost during transmission to JPL. Therefore, real time and postflight data processing

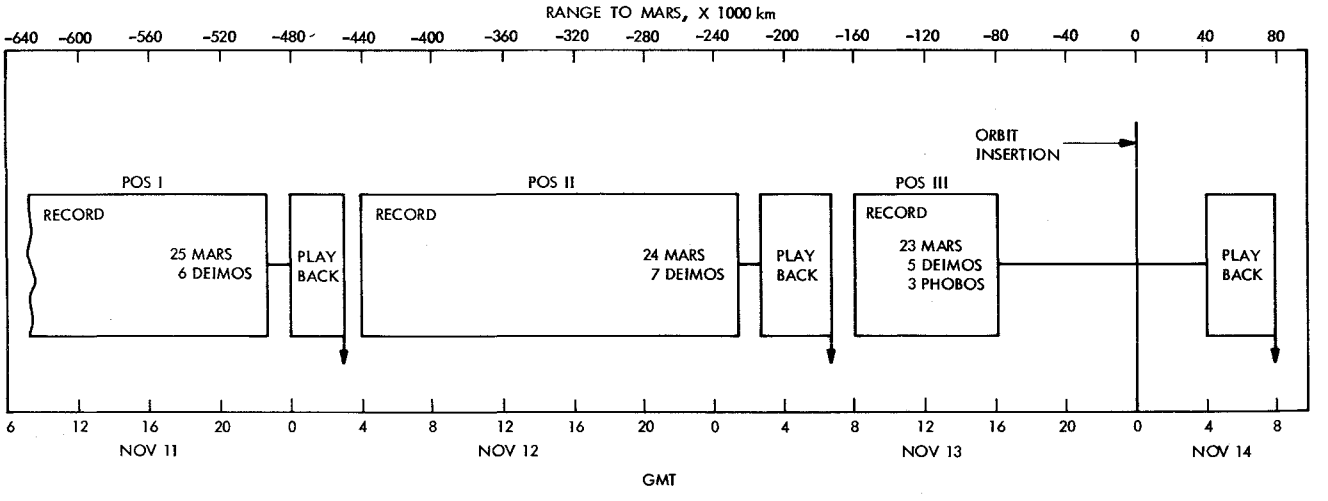

Fig. 3 Approach picture sequence.

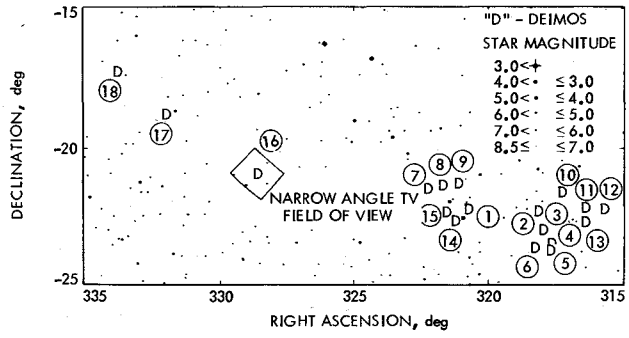

Fig. 4 Approach Deimos/star geometry.

had only five POS I pictures. Also, one of the three Phobos pictures in POS III was missed because of improper pointing of the TV camera. With only two Phobos approach pictures and large a priori Phobos ephemeris uncertainties, the Phobos data did not give any improvement of navigation accuracy over the Deimos data.

VI. Combined Doppler and Optical Solutions

Solutions which use a combination of Doppler and optical data are of particular value during planetary approach since these data types complement one another. The primary error sources prior to encounter in solutions using only Doppler data are target planet ephemeris errors, station location errors, and nongravitational accelerations. Optical data are insensitive to these errors since it directly relates the planet and spacecraft positions. On the other hand, optical data suffers from the inability to determine accurately time of flight and velocity (V_∞) of the spacecraft, quantities which, for favorable approach geometry as in the case of Mariner 9, are well determined by Doppler data. Hence, the combination of radio and optical data yields extremely accurate solutions and gives a good estimate of encounter conditions much earlier than either data type taken separately.

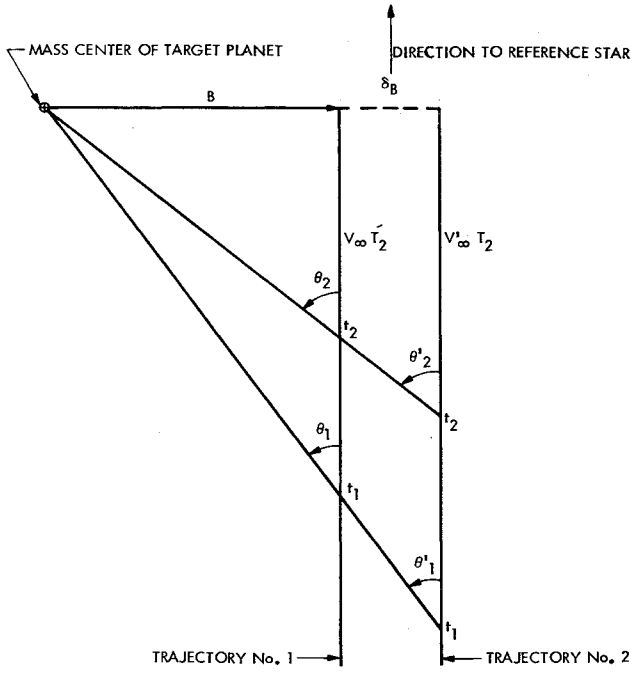

Fig. 5 Approach trajectory geometry.

Optical observations, either planet limb or natural satellites, essentially measure the angle between the target planet center of mass and a reference direction, e.g., a star direction. For the purposes of this analysis, the error in this angular measurement represents the accumulation of all error sources such as center-finding errors, satellite ephemeris errors, biases, and camera pointing errors. These errors effectively result in a degradation of the observation angle.

Assume that the spacecraft is moving on trajectory No. 1 (Fig. 5). Let θ_1 and θ_2 represent two angular measurements of the direction between the reference star and center of mass of the target planet. For simplicity the reference star is assumed to lie along the V_∞ vector. In general, the observable equation is

$$\tan\theta_i = (B/V_\infty T_i) \tag{1}$$

where $T_i = T - t_i$ and B is the magnitude of B vector, V_∞ is the velocity on the approach asymptote, T is the time of flight, and t_i is the time of ith observation.

From Eq. (1) it is seen that the time of flight, T, can be determined from two perfect observations of θ. However, only the ratio B/V_∞ can be determined from observations of θ. This is because the observation history for any parallel trajectory with the same value of B/V_∞ (for example, trajectory No. 2) will be identical to the true trajectory. These parallel trajectories also will have the same time of flight as the true trajectory. Note also that two perfect direction observations determine the plane of motion. For small values of θ_1, Eq. (1) yields

$$(\delta B/B) = (\delta V_\infty / V_\infty) + (\delta T/T) + (\delta\theta/\theta) \tag{2}$$

Consequently, even with perfect observations the limiting accuracy for B is determined by δV_∞.

Even though in theory two perfect observations of θ uniquely determine time of flight, in practice this quantity is rather poorly determined by optical data since it is extremely sensitive to errors in θ. This can be illustrated by examining an expression for the time of flight uncertainty.

Assume that two independent observations of θ are taken, the standard deviation of T becomes

$$\sigma_T = \frac{V_\infty\, T_1 T_2 (T_1^2 + T_2^2)^{1/2}}{B(T_1 - T_2)}\,\sigma_\theta \tag{3}$$

From Eq. (3) it is seen that the uncertainty in time of flight is very sensitive to the uncertainty in pointing angle when the spacecraft is far from the target planet and decreases as the spacecraft approaches the planet. Equation (3) emphasizes the importance of stars in the data since they minimize the contribution of pointing errors to σ_θ. It is seen that a larger B, which increases parallax, minimizes the error. A smaller V_∞ also gives more parallax by decreasing the range at which the observations are taken. Finally, for a fixed measurement time, T_1, Eq. (3) is minimized as T_2 is taken close to encounter.

Equation (3) also illustrates the quantities V_∞ and T which are weakly determined by optical data. Since these same quantities are generally determined very well by Earth-based Doppler data, the combination of the two data types can yield good solutions much sooner than either type used separately.

It is emphasized that the analysis presented here only applies far from encounter. As the spacecraft approaches the planet, parallax effects in the case of natural satellite observations allow one to solve for V_∞. Also the time of flight solution becomes less sensitive to pointing errors. Furthermore, sufficient data will have been taken to estimate the natural satellite's ephemeris relative to the target planet thus reducing effects of this error source. In the case of planet limb observations, V_∞ cannot be accurately determined until planetary bending of the approach trajectory occurs.

In the case of Deimos, parallax effects are discernible long before planetary bending occurs. In addition, the small size of Deimos makes image center-finding errors negligible. These two factors make satellite observation significantly more accurate than Mars limb observations for approach navigation.

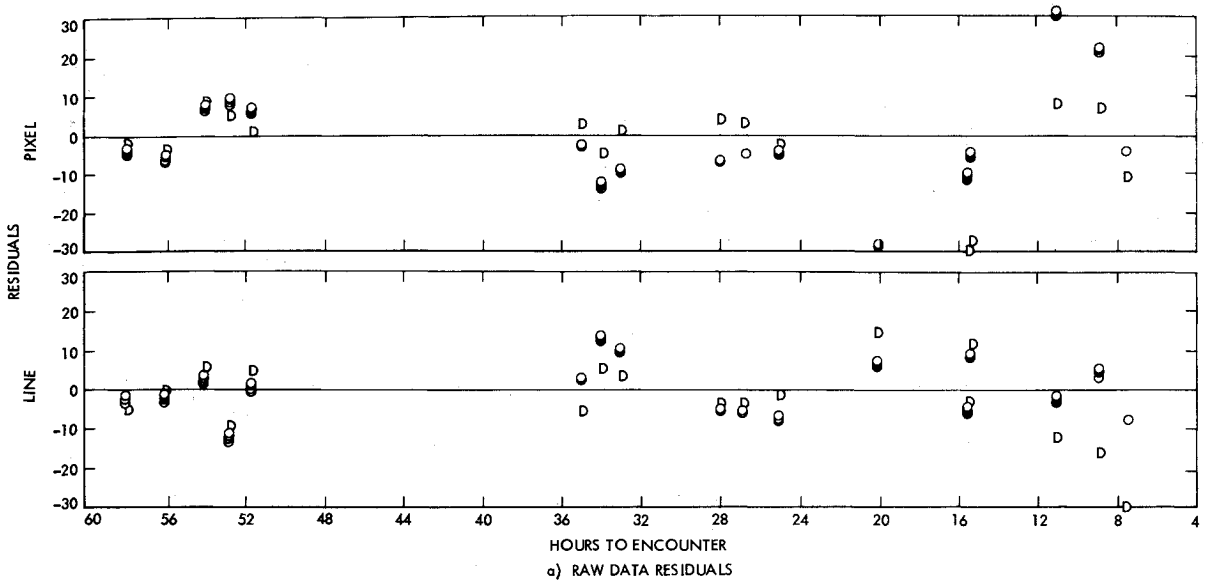

a) RAW DATA RESIDUALS

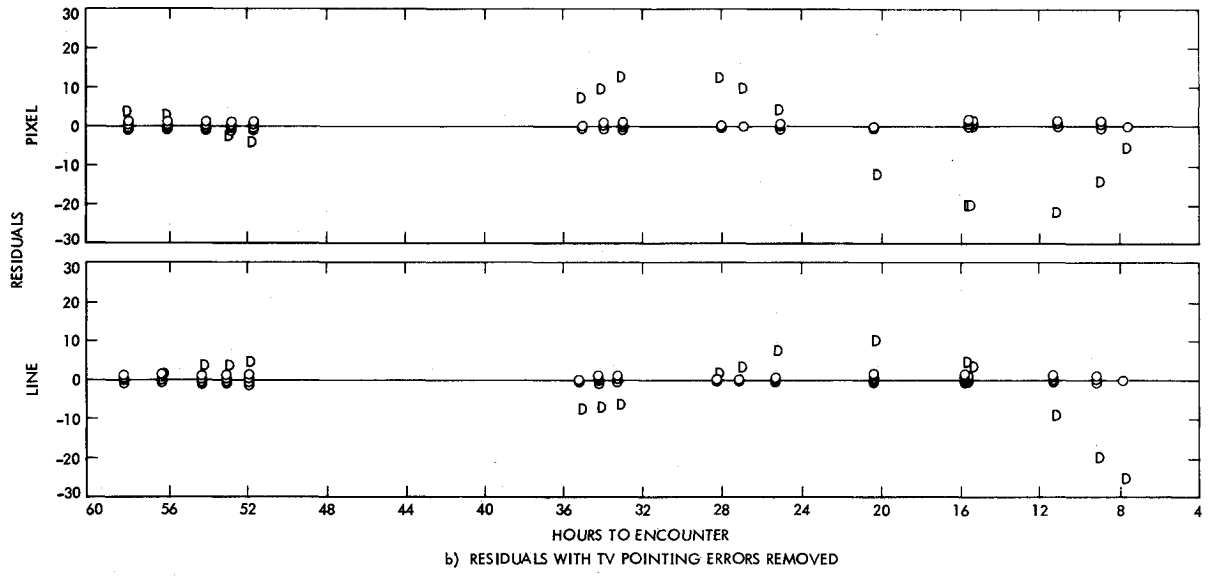

b) RESIDUALS WITH TV POINTING ERRORS REMOVED

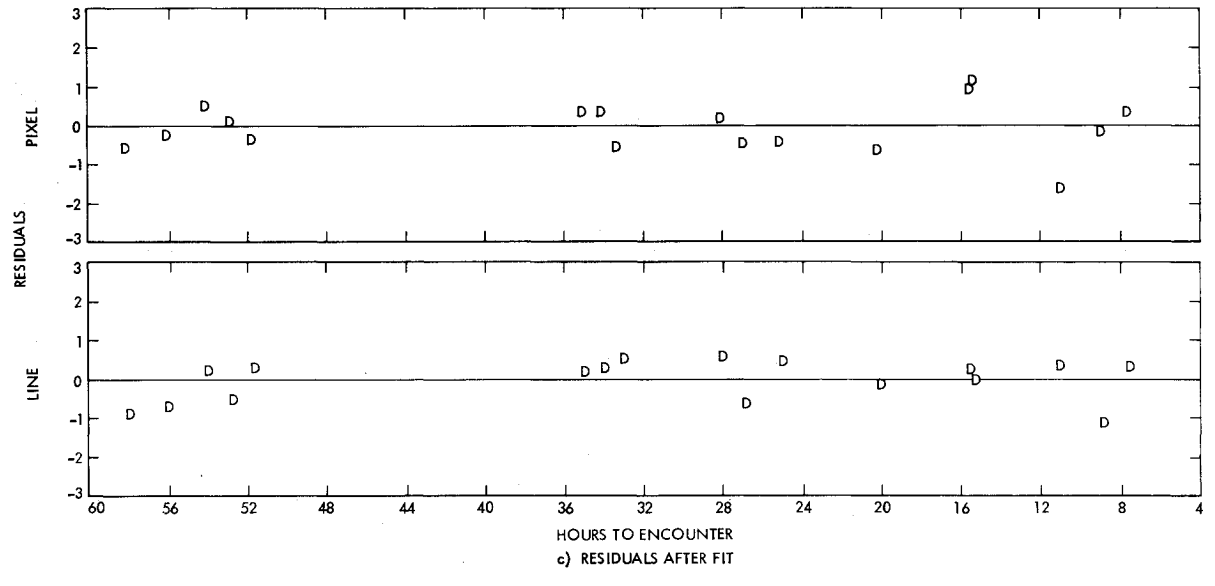

c) RESIDUALS AFTER FIT

Fig. 6 Deimos observation residuals.

VII. Techniques for Combined Solutions

Optical data were combined with a short arc (4½ days) of radio Doppler data as independent data types. A short arc of radio data is sufficient to determine the spacecraft velocity and time of flight without being corrupted by unmodeled accelerations, station location errors, and Mars ephemeris errors. Since optical data was insensitive to these errors, an accurate simultaneous solution for the state of the spacecraft and the ephemeris of Deimos relative to Mars can be obtained.

Optical data were combined with 4½ days of Doppler data which extended from November 9 to E-19 hr. The solution list contained the spacecraft state plus four elements of Deimos orbit. Since Deimos is in a near circular, near equatorial orbit, only two orientation angles, inclination and mean anomaly were included in the solution along with semimajor axis and eccentricity.

VIII. Real Time Results

During Mars approach, 12 Deimos pictures were included in the real time navigation process. Prior to obtaining these pictures, an insertion maneuver had been calculated and stored aboard Mariner 9 at E-5 days. The maneuver would only be updated in the event that additional radio data and the optical data indicated an unacceptable trajectory error. Additional radio and optical data indicated a trajectory error of only 70 km; therefore, no update to the maneuver was required. However, if the decision to update the insertion maneuver had been made, a solution based on radio plus optical data was available at E-10 hr and had an error of less than 10 km.

Optical data were processed in three iterations. In the first iteration, star images were processed to remove TV pointing errors. Pointing errors were generally large enough to introduce nonlinearities into the data processing because of the nonlinearity of the TV distortion model. In the second iteration, star and satellite images were processed. Residual TV pointing errors from linear corrections in the first iteration were removed. Also, Deimos ephemerides and the spacecraft trajectory were estimated

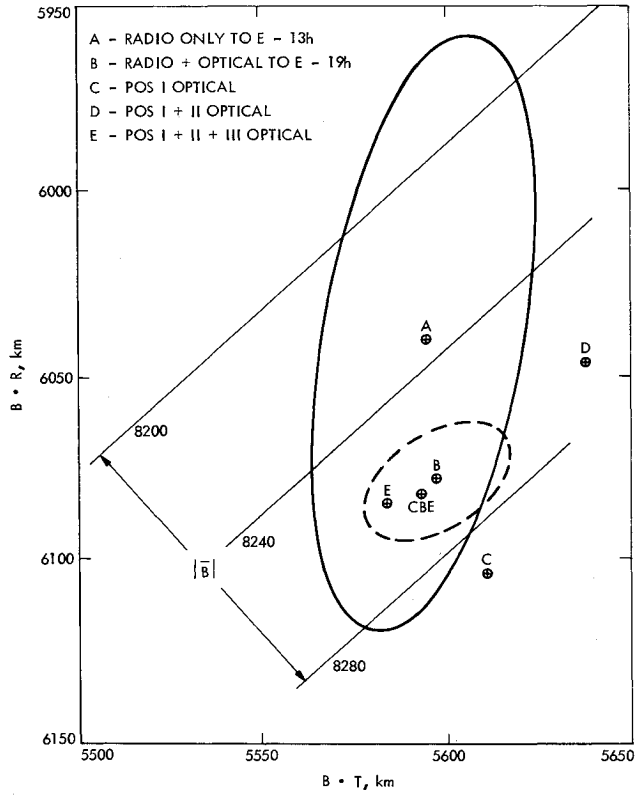

Fig. 7 Real time trajectory estimates.

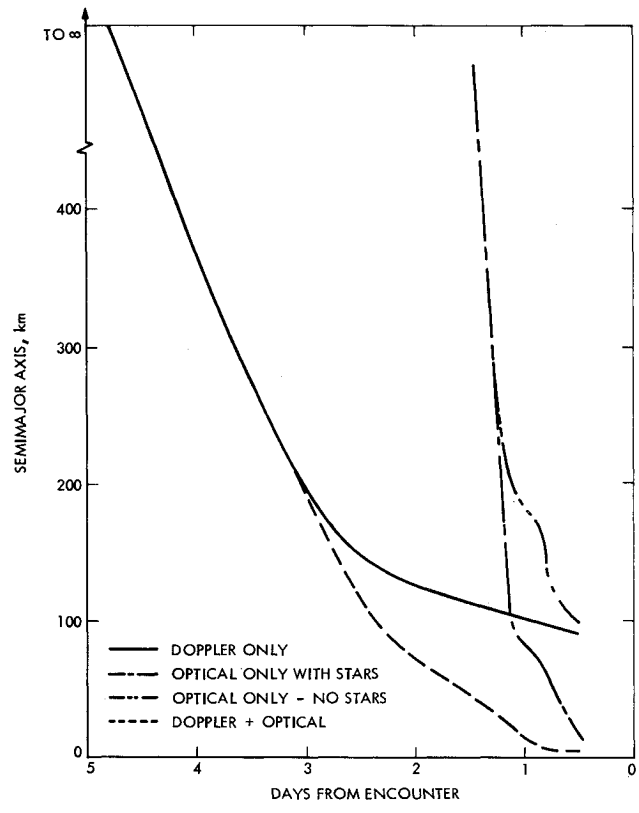

Fig. 8 Expected trajectory estimation accuracy.

to reduce Deimos data residuals within a linear region. A trajectory based on radio data only was used in the second iteration; however, a loose a priori uncertainty (thousands of km) was used. The third iteration produced combined spacecraft trajectory and Deimos ephemeris estimates using Deimos data and radio Doppler data. After a Deimos ephemeris update from POS I data, the second and third iterations could be combined.

The optical residuals (difference between observed and computed image locations) for Deimos (*D*) and stars (*o*) are shown in Fig. 6. The residuals in Fig. 6a were obtained using a priori Deimos ephemerides, a trajectory based on radio data to encounter minus 19 hr (E-19 hr), and TV pointing based on reduced spacecraft telemetry data. The clusters of star residuals reflect the global offset of the images due to TV pointing errors. It is noted that the TV pointing errors become large at the end of POS II and throughout POS III in the pixel direction but were smaller and more random in the line direction.

The residuals in Fig. 6b were generated using the same conditions as those in Fig. 6a with the exception that TV pointing errors have been removed by using the star images. Note that the star residuals which are only sensitive to TV pointing errors are zero mean. With TV pointing errors removed, the Deimos residuals reflect Deimos ephemeris errors (30-hr period) and spacecraft trajectory errors. The Deimos ephemeris errors are evident in the 30-hr periodic cycle seen in POS II and POS III residuals. The spacecraft trajectory error is seen as a slope in the line residuals.

The residuals in Fig. 6c were generated after solving for the spacecraft trajectory and Deimos ephemerides. A 300 km Deimos ephemeris error and 70 km spacecraft trajectory error were determined. Note that the residuals are zero mean and random, having a standard deviation of less than 0.5 pixels (3 arc sec).

Figure 7 shows the B-plane trajectory estimates which were generated in real time. The radio only solution and its 1σ error ellipse were based on data to E-13 hr. The radio plus optical iterated solution and 1σ error ellipse were based on radio data to E-19 hr and optical data from POS I and POS II. The current best estimate is denoted as CBE. Also, solutions denoted

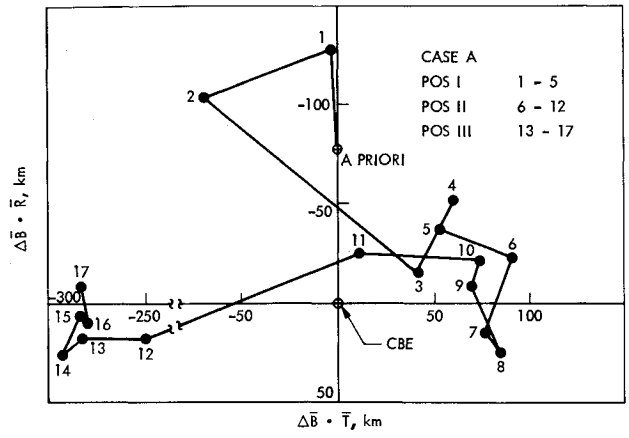

Fig. 9 Trajectory estimate using no stars.

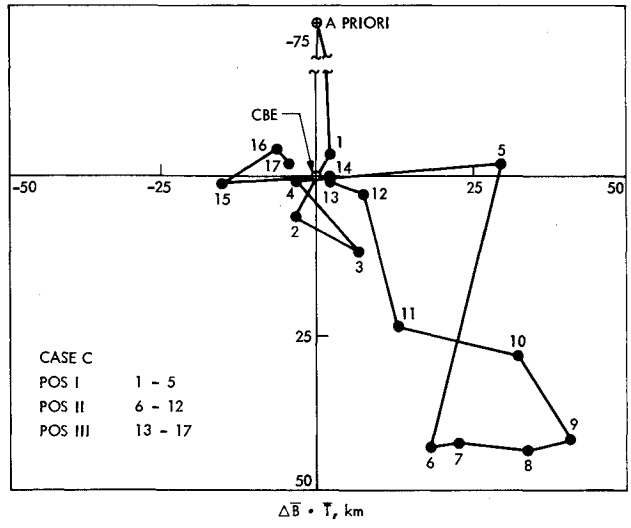

Fig. 11 Trajectory estimate using many stars/picture.

as optical were generated using a trajectory based on radio data but processing optical data only. These optical solutions were obtained from the second iteration of optical data.

Postflight evaluation of the data has given greater insight to the data and has confirmed the accuracy of the real time trajectory estimates.

IX. Sensitivity to Stars

The orbit determination (OD) accuracy sensitivity to the number of stars per picture was investigated. The following three cases were studied: A) no stars/picture, B) one star/picture, and C) an average of five stars/picture. All three cases had a priori TV pointing information from reduced spacecraft telemetry data. Also, the nominal trajectory was based on radio data only from E-30 days to E-16 hr. OD accuracies for the three cases are shown in Fig. 8 and the associated trajectory estimates are shown in Figs. 9–11.

Figures 10 and 11 show that the first picture in POS I for cases B and C drives the trajectory estimate to within 15 km of the CBE. The time behavior of cases B and C are very similar, with the trajectory estimates within 10 km agreement at the end of POS I and POS II data and within 2 km agreement at the end of POS III data. The expected accuracies of cases B and C (Fig. 8) are the same.

TV pointing derived from spacecraft telemetry is an order of magnitude less accurate than pointing derived from star images. This degradation is reflected in both the expected accuracy and the actual trajectory estimate of case A (Fig. 9) as compared to cases B and C. The case A trajectory estimate is well behaved when compared to its expected accuracy until the last picture in POS II. Then the large nonrandom TV pointing errors (modeled as random errors) in the remaining pictures drove the trajectory estimate to a 3σ error. Improved trajectory accuracy may be possible by modeling the TV pointing errors as time correlated processes.

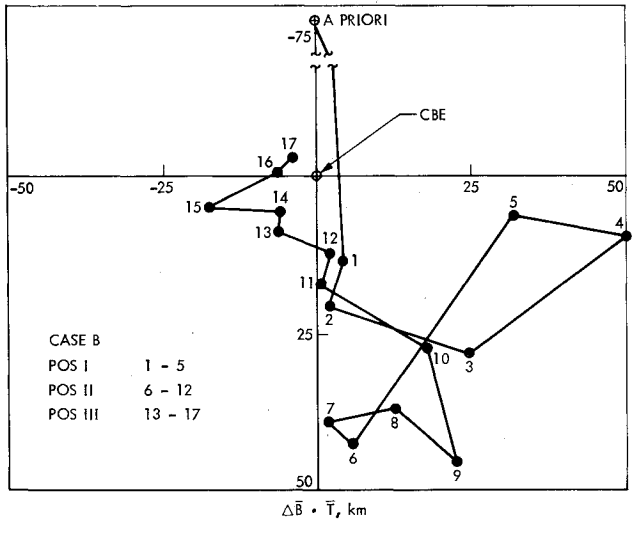

Fig. 10 Trajectory estimate using one star/picture.

The full accuracy potential of the optical data can be obtained with only one star/picture. These star sensitivity results can be explained by examining the TV pointing errors. For a given picture, all sources of pointing errors can be modeled as three independent rotations about the axes of an orthogonal coordinate system (e.g., TV pointing has three degrees of rotational freedom). One star image (a pixel and line observation) yields two of the three degrees of rotational freedom. The third degree of freedom is obtained from a second star or from a priori TV pointing which has an accuracy of a few tenths of a degree. A priori TV pointing to this accuracy can be obtained from either reduced spacecraft telemetry data ($0.015°-1\sigma$) or from the desired pointing ($0.15°-1\sigma$). Additional stars, however, do not improve the Deimos-inertial reference information in a picture. Deimos image location measurement errors control this accuracy and are not affected by star observations.

Even though only one star/picture is needed, it is desirable to have many stars/picture from a reliability standpoint. Many stars/picture give independent checks on the TV pointing and also indicate the accuracy of the TV distortion model. Any discrepancy between image location residuals within a given picture would flag it for further evaluation.

X. Sensitivity to TV Distortion

A comparison was made of navigation performance as a function of the data type used to estimate TV distortion and also the order of polynomial used to model distortion. Data used for distortion calibration included: 1) only reseau images from ground pictures, 2) only reseau images from flight pictures, and 3) only star images from flight pictures. Distortion polynomials of first (linear) and third order were compared to results from the nominal sixth-order polynomial.

In comparing calibration data, it was found that all three types gave equivalent trajectory estimation results. The TV distortion did not change from prelaunch to the end of the mission. Only a linear shift and rotation of the reseau grid of a few pixels was measured, which was easily absorbed in the TV

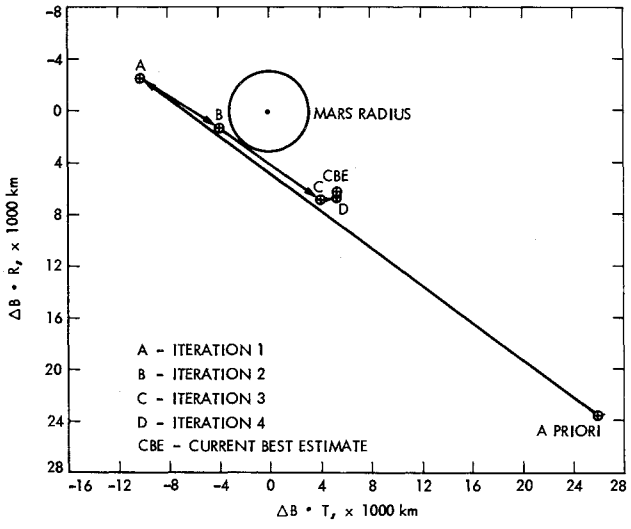

Fig. 12 Optical data trajectory solution.

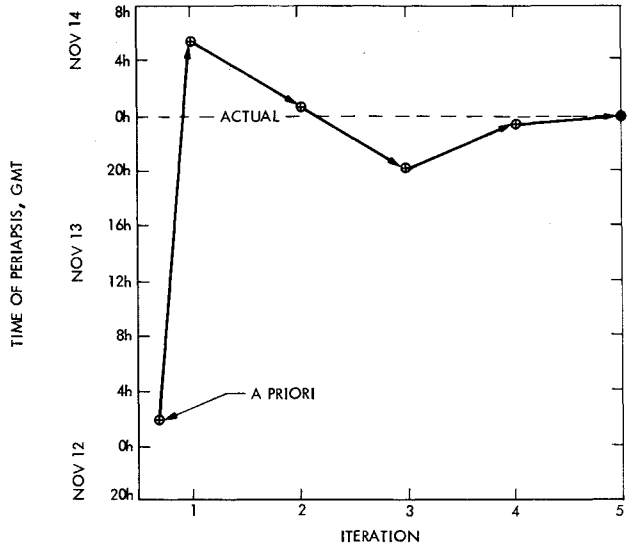

Fig. 13 Optical data flight time solution.

pointing error model. Approximately 200 star images from Plieades pictures and optical navigation pictures were used to produce equivalent results as from reseau data. Stars are a more desirable data type for distortion calibration because they also enable the calibration of optical distortion, in addition to electromagnetic distortion and are more easily detected than reseaux.

A tradeoff for increased optical data linearity at the expense of reduced model accuracy was evaluated. It was found that the linear and third-order distortion polynomial gave equivalent trajectory estimates to the nominal sixth-order model. The increased linearity was accompanied with a slightly noisier trajectory estimate behavior which, however, was well within the predicted accuracy. Therefore, it is concluded that a first-order (linear) model would suffice if time constraints would not allow iteration of the optical data. If time is available, which will generally be the case, the third-order model gives the full accuracy potential of the optical data with iteration of the data.

XI. Sensitivity to Radio Tracking Data

To evaluate the strength of optical data, a trajectory solution was made without the aid of any other tracking data. From a previous section, it is expected that POS I and II data alone would yield an accurate $\bar{B}\cdot\bar{R}$ and $\bar{B}\cdot\bar{T}$ solution but limited pictures and observed parallax would degrade the time of flight accuracy. However, POS III data containing both Deimos parallax and trajectory bending would yield a complete trajectory determination from only the optical data.

A nominal trajectory was generated from Atlas/Centaur injection conditions. These injection conditions gave a 25,000 km aim point bias at Mars for planetary quarantine. The use of this trajectory did not allow the optical data to "know," a priori, that a midcourse maneuver had been performed five days after launch. The midcourse maneuver changed the actual trajectory aim point by 15,000 km and arrival time by about a day (250,000 km). In other words, this a priori trajectory gave the optical data only a vague indication that the spacecraft was going in the vicinity of Mars. Also the preflight Deimos ephemerides having a 400 km error was used.

Initially, only POS I and II data were iterated. Only these results would have been available in real time since the POS III data was played back after insertion. Five complete iterations of the POS I and II data were needed to obtain a converged solution because of the nonlinearity due to the 250,000 km a priori trajectory error. After a converged solution was obtained for the POS I and II data, an additional solution was made which included the POS III data. This final solution allowed the full potential of the approach optical data to be evaluated.

The B-plane trajectory estimates are shown in Figs. 12 and 13 at the end of a complete iteration of POS I and II data. It can be seen that an accurate estimate of $\bar{B}\cdot\bar{T}$ and $\bar{B}\cdot\bar{R}$ can be obtained using only POS I and II data as expected. The B-plane estimate after five iterations was within 10 km and 10 sec of the current best estimate. This estimate meets mission accuracy requirements for inserting Mariner 9 into orbit about Mars. Adding the POS III data brought the B-plane estimates from optical data only to within 5 km and 3 sec of the current best estimate.

The time of flight estimate and expected uncertainty from the final solution are shown in Fig. 14. It is seen that the uncertainty does not go below a few seconds until 10 hr from encounter. This level of accuracy would be available about a day before encounter from radio metric data. It is concluded, therefore, that optical data only can yield an accurate trajectory estimate using data within 10 hr from Mars encounter. By

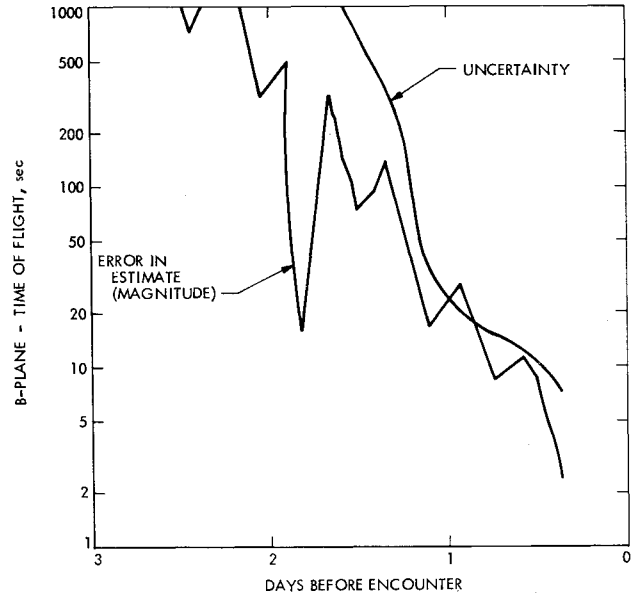

Fig. 14 Estimate of time of flight using optical data.

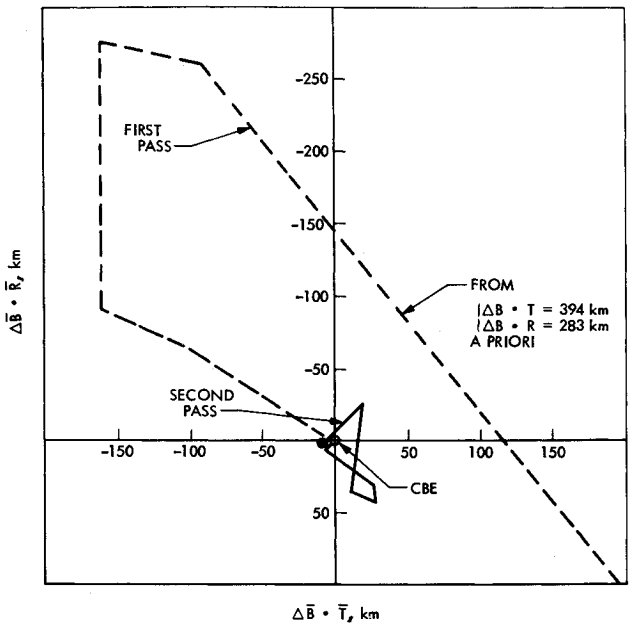

Fig. 15 Sensitivity to Mars ephemeris error.

combining optical and radio data, an estimate of comparable accuracy can be obtained much earlier.

XII. Sensitivity to Mars Ephemeris

One major source of error in the use of Doppler data for navigation estimates is planetary ephemeris errors. This results from the fact that the data are taken by stations on Earth and must be related to the target planet by using assumed station locations and a planetary ephemeris. However, from onboard optical data, the spacecraft state is directly related to the target planet. After the insertion of Mariner 9 into Mars orbit there was an update to the planetary ephemeris effecting the position of Mars by about 40 km. The optical navigation estimates for the B-plane parameters were unaffected by this change.

To demonstrate the independence of optical navigation estimates from the planetary ephemeris errors, a solution was made with a Mars ephemeris error of about 500 km. The results of processing the optical data with this ephemeris error are shown in Fig. 15, giving the B-plane solution history. The origin of the plot is at the current best estimate (CBE). The figure shows that the first pass through the data moves the estimate from an a priori more than 500 km away to within 10 km of the CBE. The final iteration moves the estimate to within 2 km of the CBE.

XIII. Conclusions

The Doppler plus satellite/star trajectory estimate for Mariner 9 was the most accurate solution generated during any real time approach operation. The new optical data, navigation techniques and science TV camera were successfully demonstrated during real time and postflight analysis. Star and reseau images were used to eliminate all systematic TV pointing and distortion errors to arc-sec accuracy. Consequently, satellite image location errors were random, having a measurement noise of 3.0 arc sec (1σ). The addition of the optical data to a few days of radio data allows the approach navigation process to reach its full accuracy potential and become insensitive to planetary ephemeris errors, nongravitational spacecraft accelerations and Earth-based tracking station location errors. Thus a demonstrated navigation capability now exists which can meet the demanding requirements of future missions such as multiple outer planet or satellite tour missions.

References

[1] Duxbury, T. C., "A Spacecraft-Based Navigation Instrument for Outer Planet Missions," *Journal of Spacecraft and Rockets,* Vol. 7, No. 8, Aug. 1970, pp. 928–933.

[2] Duxbury, T. C. and H. Ohtakay, "In-Flight Calibration of an Interplanetary Navigation Instrument," *Journal of Spacecraft and Rockets,* Vol. 8, No. 10, Oct. 1971, pp. 1038–1042.

[3] Acton, C. H., "Processing On-Board Optical Data for Planetary Approach Navigation," AIAA Paper 72-53, San Diego, Calif., 1972.

[4] Breckenridge, W. G. and Acton, C. H., "A Detailed Analysis of Mariner 9 TV Navigation Data," AIAA Paper 72-866, Stanford, Calif., 1972.

[5] Duxbury, T. C. and Acton, C. H., "On-Board Optical Navigation Data from Mariner '71," Institute of Navigation—National Space Meeting, March 1972.

[6] Aksnes, K., "On the Use of Hill Variables in Artificial Satellite Theory: Brouwer's Theory," *Journal of Astronomy and Astrophysics,* Vol. 17, No. 70, 1972, pp. 70–75.